Impact of Asian orography on ENSO

Author: Victòria Agudetse Roures
Supervisor: Dr. Ileana Bladé Mendoza, ileanablade@ub.edu
Facultat de Física, Universitat de Barcelona, Diagonal 645, 08028 Barcelona, Spain.

Abstract: Tall mountain ranges such as the Tibetan Plateau and the Rocky Mountains play a significant role in shaping the climatological Northern Hemisphere zonal wind distribution and the stationary waves in the geopotential field. In this work we assess the influence of Asian orography on ENSO and its wintertime teleconnections by comparing a flattened-orography simulation to a control simulation using an ocean-atmosphere coupled model. We have found that the presence of the Asian orography is key to both ENSO and its teleconnection pattern. When the mountains are not present, El Niño and La Niña events decay more rapidly and the ENSO cycle has a higher frequency, is more regular, and is characterized by stronger sea surface temperature anomalies. The Northern Hemisphere winter teleconnection pattern in the geopotential field also changes significantly, with a new Rossby wave train emerging from Southern Asia and propagating northwestward, and a ridge appearing over Greenland.

I. INTRODUCTION

El Niño-Southern Oscillation (ENSO) is a coupled ocean-atmosphere phenomenon that is responsible for a high proportion of the interannual variability in the tropical Pacific ocean sea-surface temperature (SST). The atmospheric aspect of ENSO, called the Southern Oscillation, is characterized by a sea-level pressure dipole pattern with centers in the Western Pacific Ocean (Indonesia) and the Eastern Pacific (Tahiti). This pattern is correlated with SST anomalies in the Eastern and Central Pacific ocean and off the coast of Perú. Thus, anomalously low pressures over the Eastern Pacific and high pressures in the Western Pacific are associated with a warming in the central and eastern equatorial Pacific ocean (a region known as the cold tongue for its normally cool SST conditions). This warming is caused by a weakening of the trade winds, which leads to reduced upwelling of deep cold water, a deeper thermocline and reduced evaporative cooling (*Rasmusson and Carpenter* 1982). This warm phase of the oscillation is known as El Niño, while the opposite phase of anomalous cooling is called La Niña. In-between conditions with SSTs close to the climatological mean are said to be neutral.

'Teleconnection' is a term commonly used in the literature to describe patterns of simultaneous fluctuations between variables (e.g. SLP or geopotential height) separated by long distances (*Wallace and Gutzler* 1981). The Southern Oscillation itself is one such pattern, with the behavior of a standing oscillation, and an irregular time scale of 2 to 8 years (*Rasmusson and Carpenter* 1982).

In addition to this main see-saw pattern in the tropics, other documented teleconnection patterns that extend into the extratropics are also associated with ENSO. The changes in sea level pressure and sea surface temperature associated with the warm and cold phases of the cycle trigger changes in the distribution of tropical convection and upper level divergence, which in turn modify the extra-tropical atmospheric circulation as anomalies propagating poleward with the form of atmospheric Rossby waves. In the presence of localized midlatitude jets and meridional vorticity gradients, these Rossby wave patterns can be relatively insensitive to the specific longitude of the anomalous warming (*Horel and Wallace* 1981), (*Trenberth et al.* 1998), (*Hoskins and Karoly* 1981).

These teleconnections are strongest in winter because the stronger westerly winds in the midlatitudes favor their propagation from the tropics to the extratropics (*Trenberth et al.* 1998), (*Horel and Wallace* 1981), (*Held et al.* 2002). They are also stronger in the Northern Hemisphere, where the patterns tend to be more robust, as the weaker Southern Hemisphere teleconnections are more easily masked by natural variability (*Trenberth et al.* 1998).

The characterization of the NH winter ENSO teleconnection is somewhat controversial as it resembles both the Pacific-North American (PNA) and the Tropical/Northern-Hemisphere (TNH) teleconnection patterns. The PNA is a midlatitude tropospheric teleconnection pattern with four centers of alternating anomalous ridges and troughs: one in the subtropical Pacific near Hawai'i, one over the North Pacific Ocean, another over western Canada, and the fourth one reaching the east coast (Gulf Coast region) of the United States (*Wallace and Gutzler* 1981). The sign of this pattern is defined positive during the months of strong ridging over western Canada, as shown schematically in Fig.(1). Although it is a natural mode of internal variability within the atmosphere, its positive phase is associated with El Niño years while the negative phase commonly occurs in La Niña years (*Horel and Wallace* 1981).

The negative phase of the TNH, which tends to be present during El Niño years, is characterized by positive anomalies over the tropical Pacific and the northern half of North America, and negative anomalies over the North Pacific and over the Atlantic off the East Coast of the United States (*Mo and Livezey* 1986).

Large mountain ranges are essential to the distribution of air masses and stationary troughs and ridges in the middle and upper troposphere. Acting as obstacles due to their vertical and meridional extensions, they alter the

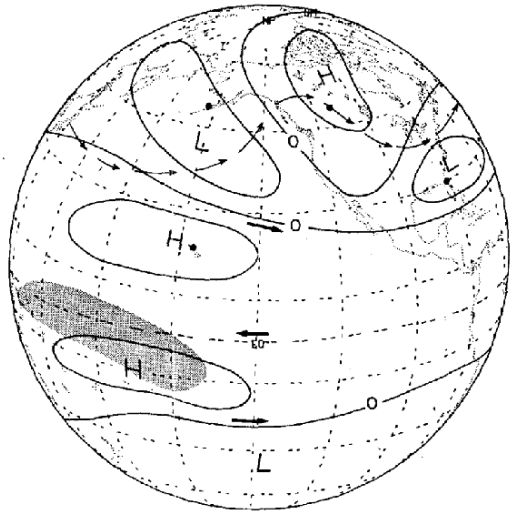

Figure 1: Schematic illustration of the Pacific-North American teleconnection pattern which is associated with the warm phase of ENSO in winter. From *Horel and Wallace*, 1981.

zonal flow and give rise to wave patterns downstream (*Bolin* 1950). The distribution of mid-latitude westerly winds and the location of the subtropical jet stream are highly influenced by these large barriers in the middle latitudes.

Studies on the impact of mountains on Earth's climate flourished in the mid 20th century with the development of climate models that enabled scientists to design and perform experiments with modified orography and compare the state of the atmosphere to that of an unmodified Earth. Models with multiple vertical levels showed that, while thermal effects of heat sources and sinks dominate near the surface, the importance of orography for reproducing the main climatological features of the planet increased with height. (*Bolin* 1950), (*Manabe and Terpstra* 1974).

In the Northern Hemisphere, the Rocky Mountains and the mountain chains in the interior of Asia have the greatest influence. The Tibetan Plateau is important for the intensity and location of the Siberian high, and also enhances the north Pacific subtropical high: the deflection of the impinging westerly wind induces an anticyclonic anomaly north of the orography, a cyclonic anomaly to the south, and a wave-like response downstream. High in the troposphere, a stationary trough with a southeast-to-northwest tilt is located in the lee of these major mountain ranges, with an area of maximum westerlies to the east of the trough (*Manabe and Terpstra* 1974). Although in the Southern Hemisphere the effect of the mountains is smaller due to the lack of large-scale ranges in the midlatitudes, the Andes do have an influence on the mean flow. This effect is particularly important because the subsidence of dry air on the lee side of the Andes cools the surface in the southern tropical Pacific. This is why the Intertropical Convergence Zone is generally located north of the Equator (*Takahashi and Battisti* 2007).

Recently, (*White et al.* 2017) studied the impact of Asian orography on the Pacific wintertime circulation. The authors not only confirmed that the presence of the Tibetan and Mongolian mountains strengthens the subtropical Pacific jet stream, but also found the strongest contribution to this effect is not due to the taller Himalayas, but to the Mongolian Plateau.

Using these findings as a starting point, this TFM aims to be a preliminary study of the influence that the central Asian orography might have on the ENSO cycle and the extratropical impacts of ENSO. Section II includes a description of the datasets and analysis methods employed in this study. In Section III.A we compare the pattern of SST anomalies, periodicity and NH teleconnection pattern of ENSO in the model we use to observations. Section III.B describes the impact of removing the mountains on the ENSO cycle itself by comparing this control simulation to a simulation where Asian orography has been flattened, while Section III.C focuses on the differences in the Northern Hemisphere winter teleconnection patterns between the simulation with mountains and the simulation without, with emphasis on upper tropospheric circulation anomalies. In Section IV we outline the conclusions.

II. DATA AND METHODOLOGY

Two simulations with an ocean-atmosphere global circulation model are used: a 1000-year control simulation (CTL) and a 300-year simulation (NO_MT) where the areas encompassing the Mongolian Plateau (38.0°N to 60.0°N, 65.0°E to 152.5°E) and the Tibetan Plateau (10.0°N to 42.0°N and 62.0°E to 125.0°E) have been flattened to 50 m above mean sea level. A map of the flattened orography is shown in Fig.(2).

The atmospheric model is the Community Atmosphere Model (CAM4) coupled with the Parallel Ocean Program (POP), with a horizontal resolution of 1.9° x 2.5° and 26 vertical levels. Available output includes surface temperature and sea-level pressure, as well as geopotential height, zonal wind and meridional wind at pressure levels ranging from 1000 hPa to 10 hPa. The first 500 years of the CTL simulation are discarded as a spin-up period to allow for adjustment in ocean dynamics.

The control simulation is first compared with observational data in order to ensure that the main features of ENSO are well represented by the model. The NCEP/NCAR Reanalysis Monthly Mean data was used for the analysis of 200 hPa geopotential height. The NOAA Extended Reconstructed Sea Surface Temperature (ERSST) version 5 data was used for the analysis of SST. Both datasets were provided by the NOAA/OAR/ESRL PSD, Boulder, Colorado, USA, from their website at `http://www.esrl.noaa.gov/psd/`.

In this study, several diagnostics techniques are used to

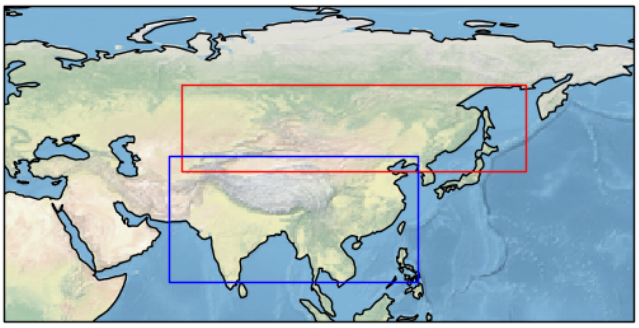

Figure 2: Areas of flattened orography in the NO_MT simulation. Red box: Mongolian Plateau. Blue box: Tibetan Plateau.

examine the differences between the simulations. Northern Hemisphere winter (December-January-February) anomalies computed from monthly data are analyzed after removing the climatological mean and applying a linear detrending function. A land mask was applied to the surface temperature data to remove land temperature variability.

Empirical Orthogonal Function (EOF) analysis is performed in order to detect the spatial and temporal pattern of SST anomalies in the tropical Pacific ocean for each set of data and compare them to each other. EOFs are defined as the eigenvectors of the covariance matrix between grid points (*Wilks* 2011). EOF analysis allows us to find spatial patterns, known as empirical orthogonal functions, that represent recurrent uncorrelated physical modes of variability within a dataset, along with the projections of the eigenvectors onto the data, which are known as principal components. Each mode is also identified by an eigenvalue that is proportional to the fraction of the total variance explained by the mode. For this analysis, each grid point is weighted by multiplying it by the square root of the cosine of its latitude.

For tropical Pacific SST, the leading EOF (the mode with the highest eigenvalue) represents the variability associated with the ENSO cycle. For both model and observational data, the leading mode is found to be statistically significant according to the criterion that its eigenvalue must be sufficiently distant from the nearest eigenvalue when considering sampling error (*North et al.* 1982). This means that the leading pattern is robust to sampling variability. From this point on we will refer to the spatial patterns as "EOFs" and to their time series as "PCs".

Regression maps are computed by correlating the data fields with the PC time series and scaling the result by the standard deviation of the field at each grid point. A two-sided student t-test is applied to check for statistical significance of these correlations at the 0.05 level.

To assess the periodicity and regularity of the ENSO cycle we use a Fast Fourier Transform algorithm to perform spectral analysis of the PC time series.

All of the data analysis is performed with Python scripts. The Python package `windspharm`, created by Andrew Dawson, is used for the computation of variables that require derivatives of the vector wind field defined on the Earth sphere in a spherical harmonic basis, such as divergence and vorticity.

III. RESULTS

A. Model ENSO vs. observed ENSO

In order to identify the pattern of variability associated with ENSO, EOF analysis is performed on the winter (DJF) mean sea surface temperature data.

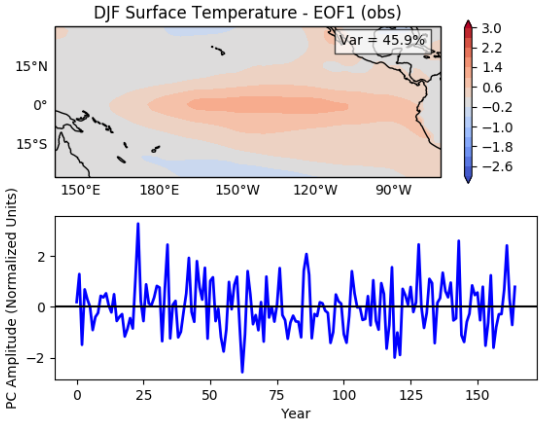

Figure 3: Leading EOF (top) and PC (bottom) for DJF mean tropical Pacific SST in the NOAA ERSST dataset, from 1854 to 2018. Units in °C.

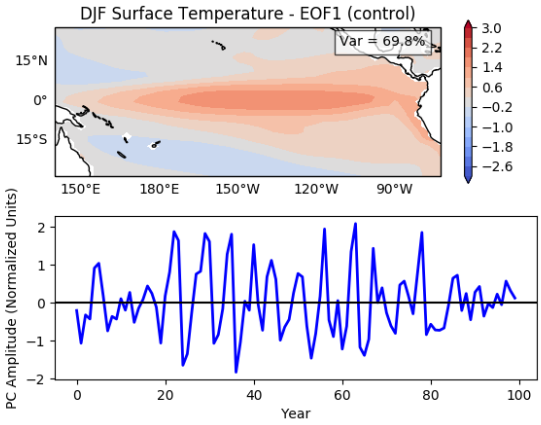

Figure 4: Leading EOF (top) and PC (bottom) for DJF mean tropical Pacific SST in the CTL simulation. Units in °C.

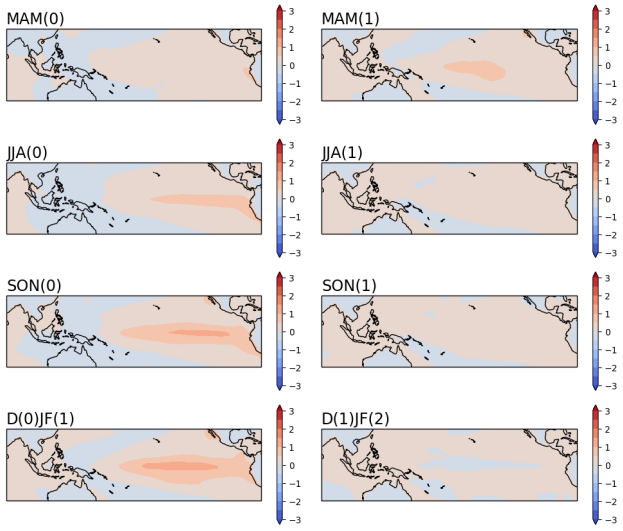

Figure 5: Lagged regressions of observed tropical SST against the PC1 time series for the 1854-2018 period. Units in °C.

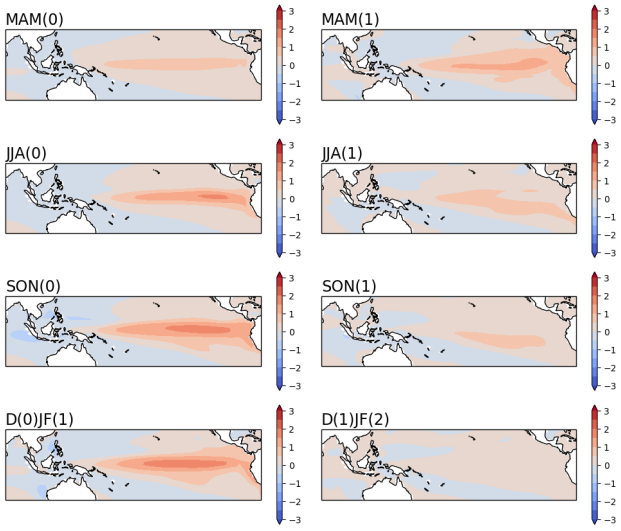

Figure 6: Lagged regressions of tropical SST against the PC1 time series for the CTL simulation. Units are °C.

Fig.(3) shows the leading EOF and PC for observational data. ENSO explains 45.9% of the variance in SST in the tropical Pacific for the 164-year time period of the ERSST dataset. For the positive phase of the pattern, there is anomalous warming along the Equator that begins just off the South American coast and extends westward up to the Date Line. The area of maximum warming is located in the 110°W-170°W band, with values around 1.5°C. The PC time series shows the irregularity of the cycle and the strong variability in the intensity of the warm and cold events. The correlation coefficient for PC1 and the Niño3.4 index (commonly used to define El Niño and La Niña events) is 0.96. The Niño3.4 index is the average SST anomaly computed over the 5°N-5°S, 170°W-120°W area box (*Trenberth and National Center for Atmospheric Research Staff, eds.* 2018).

Fig.(4) is the same as Fig.(3) for the CTL simulation of the model, but for clarity only a 100-year section of the PC time series is shown. The leading EOF in this case explains a higher percentage of the variance: 69.8%. The proportion of explained variance is statistically significantly larger in the observations according to Fisher's F-test for variances. The leading PC (PC1) is highly correlated with the model Niño3.4 index, with a correlation coefficient of 0.99. The spatial pattern is very similar to the observations and the maximum values of the warming as well, although the positive anomalies extend further west in the model.

The evolution of a typical El Niño event is shown by performing lagged regressions of tropical Pacific SST against the DJF PC time series. Fig.(5) shows that the warming peaks in intensity in the winter and then decays until temperatures reach near-normal conditions by the following fall. The decay of the simulated ENSO, shown in Fig.(5) is slower than the decay of the observed ENSO.

We more accurately compare the periodicity of the model ENSO to that of the observations through the power spectra of their respective PC1 time series, shown in Fig.(7). The spectrum for each series is an average of the spectra computed over 25-year long segments. This is done to increase the degrees of freedom in each specral estimate. Each segment is detrended and a Hann function is applied as a tapering window in order to remove discontinuities at the beginning and end points. The discrete Fourier transform is then computed and scaled, and the resulting relative values of the Power Spectral Density show the proportion of variance in each original time series that is accounted for by oscillations at each frequency.

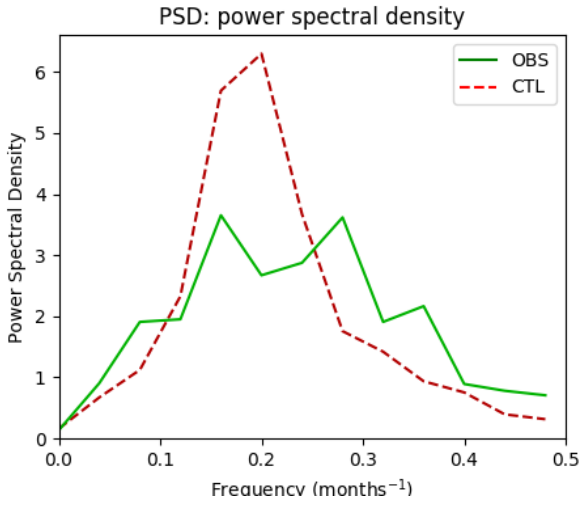

Figure 7: Power spectra of the observational dataset (green) and the CTL simulation (red). The spectra are averages of split realizations of 25 years each.

For the observational data there is a widespread peak ranging from approximately 2 to 8 years, which reflects the irregularity of the oscillation. The CTL simulation has narrower peak, with a preferred period of 5 years, indicating that the observed ENSO and the model ENSO have similar periodicity, but the model ENSO is much more regular.

Lastly, we compare the observed Northern Hemisphere teleconnections to those in the model through the regression maps in Fig.(8). These regressions show the typical anomalies in the 200 hPa geopotential height field when the tropical SST anomalies are equal to one standard deviation. In the North Pacific sector, the spatial pattern takes the form of a Rossby wavetrain emerging from the tropical Pacific, with four centers that resemble the positive phase of the PNA as illustrated schematically in Fig.(1). The simulated pattern is similar the model overestimates the magnitude of the anomalies, and a trough appears at about 30°N in Asia that is not present in the observations.

B. Impact of topography on tropical response

We now examine the same features of the ENSO cycle for the NO_MT simulation and compare them to the CTL simulation to determine if the mountains have an impact on the tropical response itself.

Fig.(9) shows the leading EOF for tropical SST in winter for the NO_MT simulation. Comparing it to Fig.4 one can see that the leading EOF shows a similar spatial pattern in the CTL and NO_MT simulations, although the temperature anomalies in the eastern Pacific region appearing to be stronger in the NO_MT case, with maximum values exceeding 3°C. For the NO_MT simulation, the leading EOF explains 77.5% of the variance and has a correlation coefficient of 0.98 with the Niño3.4 index. This mode also explains a high amount of the variance compared to both the observations and the CTL simulation. The difference between the NO_MT EOF1 and the CTL EOF1 is statistically significant.

While the spatial distribution of the anomalous warming is relatively similar, with the maximum warming over the same area, it is clear from the time series in Fig.(9) that there are important changes in the periodicity, regularity and amplitude of El Niño. Although only 100 years are shown, this is true for the entire 300-year period of the simulation. The oscillation appears to have a much more regular period and amplitude, as well as a higher frequency. In the lagged regressions for the NO_MT simulation, shown in Fig.(10), near-neutral conditions return earlier compared to the CTL, and negative anomalies exceeding -0.5°C are present by the following winter.

To better analyze those differences, a spectral analysis of the PC1 time series is performed. Power spectra are computed for 50-year chunks of the time series for all 300 years of the NO_MT run and the last 500 years of the CTL run. This is done in order to see whether

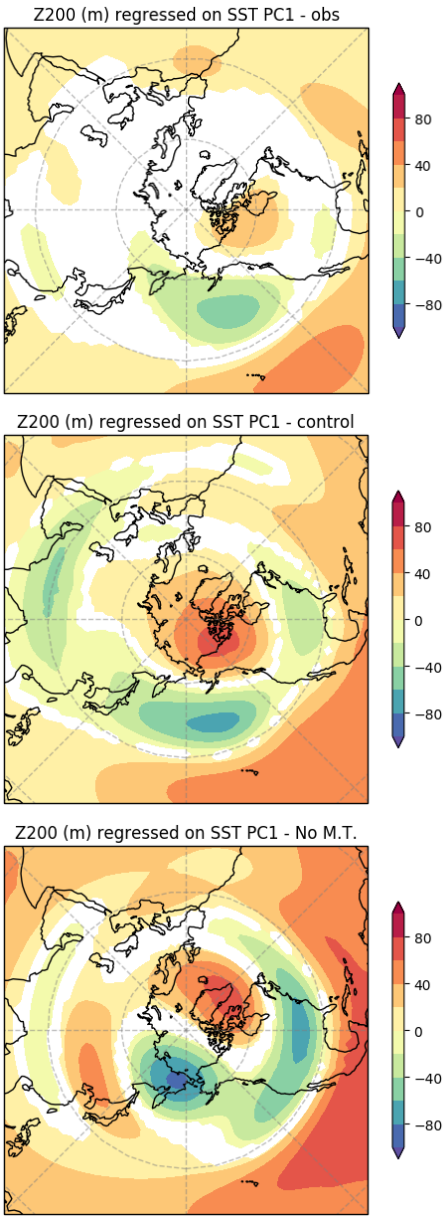

Figure 8: Regression of 200 hPa geopotential height anomalies against the PC1 time series for observations (top), CTL simulation (middle) and NO_MT simulation (bottom). Only areas where the correlation is significant at the 95% level are plotted.

the differences in both simulations could be attributed to sampling variability. In this case we use longer segments in order to have higher frequency resolution. This results in ten 50-year spectra for the CTL and six 50-year spectra for the NO_MT, which are shown in Fig.(11).

Many of the individual power spectra for the control run (area shaded in light red) exhibit enhanced variance over a wide range of frequencies, often with one or more secondary peaks present. This similar to the irregular behaviour of ENSO in nature, as seen in section III.A. In contrast, the power spectra of the NO_MT run have

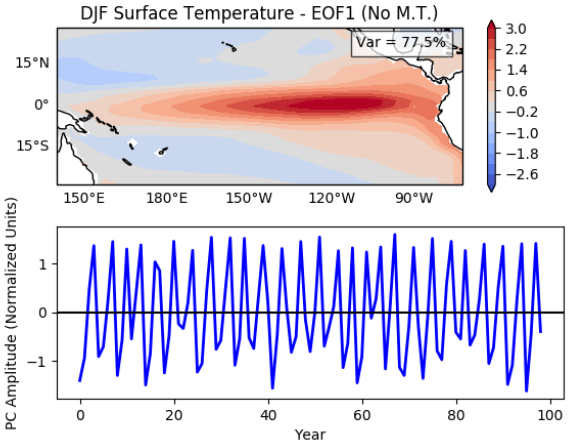

Figure 9: Leading EOF (top) and PC (bottom) for DJF mean tropical Pacific SST in the NO_MT simulation. Units are °C.

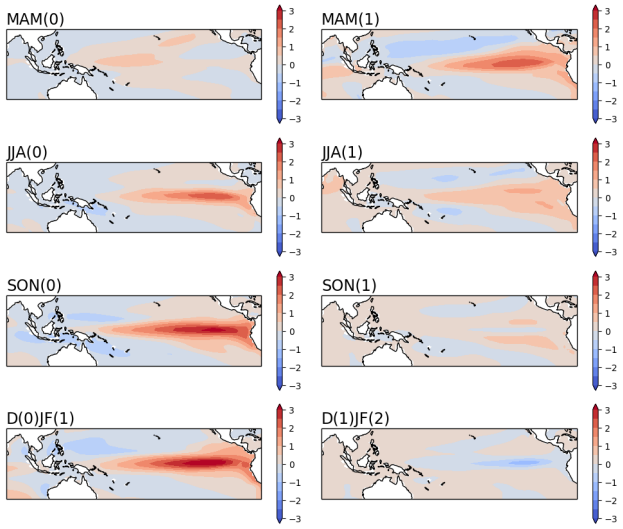

Figure 10: Lagged regressions of tropical SST against the PC1 time series for the NO_MT simulation. Units are °C.

exhibit much narrower and higher frequency peaks. For the CTL run the mean preferred period is 5 years, ranging from 3.6 to 8.3 years. The NO_MT run has a mean preferred period of 4 years, ranging from 3.8 years to 4.5 years. This suggests that Asian orography plays a role in disrupting the regularity of ENSO and shifting its timescale towards lower frequencies.

It has been hypothesized that the irregularity of the ENSO cycle may be explained by stochastic forcing from large-scale synoptic atmospheric transients such as the Madden-Julian Oscillation (MJO), a weekly-scale fluctuation in tropical weather, and associated westerly wind bursts (*Kestin et al.* 1998), (*Capotondi et al.* 2018), (*Kleeman* 2008). Recent studies suggest that the Tibetan Plateau and Himalayas have an impact on these (*Yang*

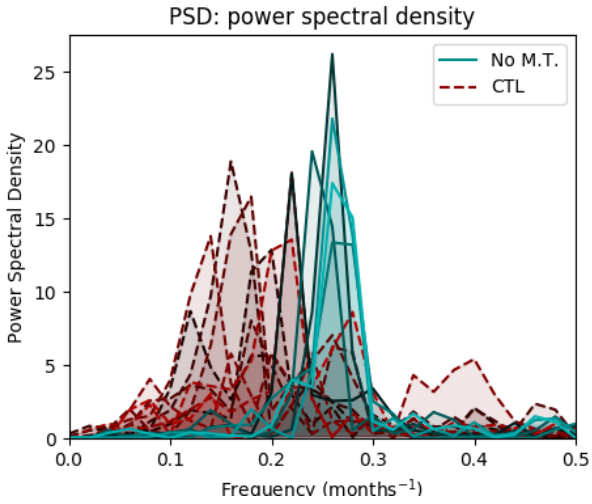

Figure 11: Power spectra of CTL and NO_MT simulations. Each spectrum corresponds to a 50-year period of the corresponding simulation. The area under each curved is shaded in red (CTL) or blue (NO_MT).

and Wang 2019). Westerly wind bursts weaken the divergent Ekman transport along the equatorial Pacific, suppressing the upwelling of deep colder water and thus favouring the development of El Niño conditions. Analogously, easterly wind bursts intensify divergent Ekman transport, initiating the return to ENSO neutral conditions or la Niña episodes. The difference in the climatology of the low-level winds in the tropical Pacific is shown in Fig.(12). The eastern equatorial Pacific surface trade winds are weaker in the NO_MT DJF climatology. Thus, the Ekman transport is weaker, and consistently climatological SSTs (not shown) are up to 1°C warmer in that area.

Westerly wind bursts may be weaker or less in the absence of the Asian mountains, and this might explain the enhanced regularity we have found in the NO_MT simulation. However, as westerly wind bursts are daily-scale events, and we only have monthly data available, we do not explore this further.

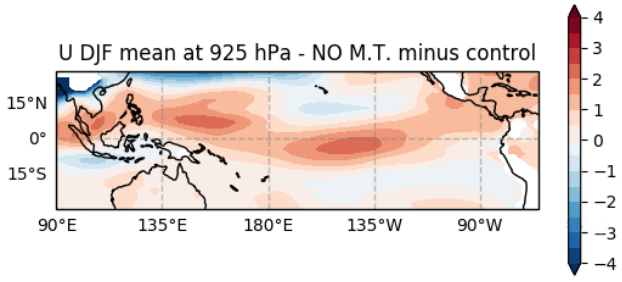

Figure 12: NO_MT minus CTL for the 925 hPa zonal wind DFJ climatology in the tropical Pacific sector. Units are m/s.

C. Impact of topography on NH winter teleconnections

To assess the role of the Mongolian and Tibetan Plateaus on the teleconnections associated with ENSO, we compare regressions of the NH winter mean sea level pressure and 200 hPa geopotential height as well as other variables that can help us understand the dynamics of the observed teleconnections.

The NO_MT teleconnection pattern, shown in Fig.(8), retains the low pressures over the south-western US but has an otherwise very different distribution of high and low pressure centers. The trough over the northern Pacific ocean disappears, with another appearing between north-eastern Russia and Alaska instead, and the Canada ridge is displaced towards Greenland. In addition to the wavetrain emerging from the eastern tropical Pacific, a second wavetrain seems to be emerging from Southern Asia and travelling north-eastward following a path that resembles a great circle. We have determined that the differences with respect to the CTL in those areas are statistically significant at the 0.05 level using a two-sample z-test.

To attempt to explain those differences, we examine the chain process by which the atmospheric perturbations caused by SST anomalies develop. The extratropical response to large-scale tropical convection can be understood in terms of anomalous planetary wave propagation from regions of tropical upper tropospheric divergence (*Hoskins and Karoly* 1981). During an El Niño event, the anomalous SST warming forces enhanced convection in the tropical Pacific ocean. This results in anomalous divergence in the upper troposphere that compensates for the increased ascent of air. To maintain the balance in the local Hadley circulation, there must also be stronger descent and convergence in the subtropics. As a consequence, twin anticyclonic anomalies develop at about 15º in both hemispheres. In the presence of mean westerly flow, these anomalies can propagate poleward and eastward into the extratropics in the form of a Rossby wavetrain (*Trenberth et al.* 1998). The vertical structure of these geopotential height anomalies is baroclinic (i.e., they change sign with height) in the tropics but equivalent barotropic in the extratropics.

The typical SST anomaly pattern as given by the leading EOFs in Fig.(4) and Fig.(9) is similar in both cases, although in the NO_MT simulation the warming is more intense in the 150ºW-90ºW longitude band. Therefore, it would be expected that this similar warming pattern would lead to similar spatial patterns of anomalous tropical convection across the Pacific ocean (*Hoskins and Karoly* 1981). Since this is not the case, we examine the upper tropospheric response to the SST anomalies in more detail.

The state of the atmosphere in the extratropics impacts the propagation of Rossby waves, and thus we first examine the climatological upper-level zonal wind. Fig.(13) shows the mean winter 200 hPa zonal wind in the CTL simulation, while Fig.(14) shows the difference in climatological wind between both simulations. The changes are mostly limited to the Northern Hemisphere. The mountains strengthen the jet stream over the western Pacific, but decrease the strength of the flow along the 30º-45º latitude band over the Asian continent. This is consistent with the results obtained in another study describing the impact of Asian orography (*White et al.* 2017), where fixed SST experiments were used to show that this impact on the winter Pacific jet stream is mostly caused by the Mongolian Plateau, rather than the taller Tibetan Plateau. There are differences in the tropical winds as well, with the NO_MT run showing a weakening of the Eastern Pacific westerly duct, a region of mean upper tropospheric equatorial westerly winds that is important for the interaction between the tropics and the extratropics, as Rossby waves can only propagate in mean westerly flow.

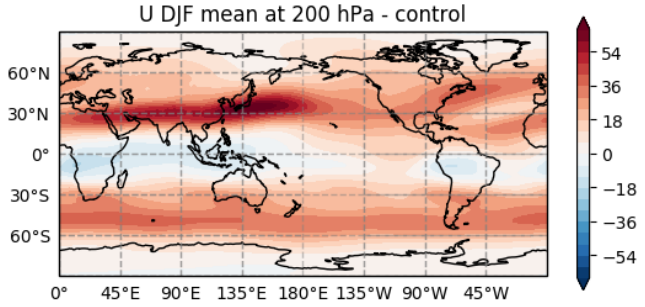

Figure 13: 200 hPa zonal wind DJF climatology for the CTL simulation. Contour units are m/s.

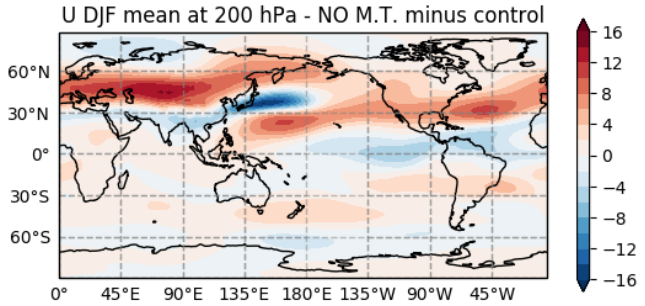

Figure 14: NO_MT minus CTL for the 200 hPa zonal wind DFJ climatology. Units are m/s.

Because we did not have access to precipitation data for both simulations, other quantities derived from the upper tropospheric wind field are used instead as a proxy for convection. In particular, the wind can be expressed as the sum of its irrotational and divergent components, such that:

$$\vec{v} = \vec{v}_\psi + \vec{v}_\chi = \vec{k} \times \nabla\psi + \nabla\chi, \tag{1}$$

where ψ is the streamfunction and χ is the velocity potential. Velocity potential describes the divergent com-

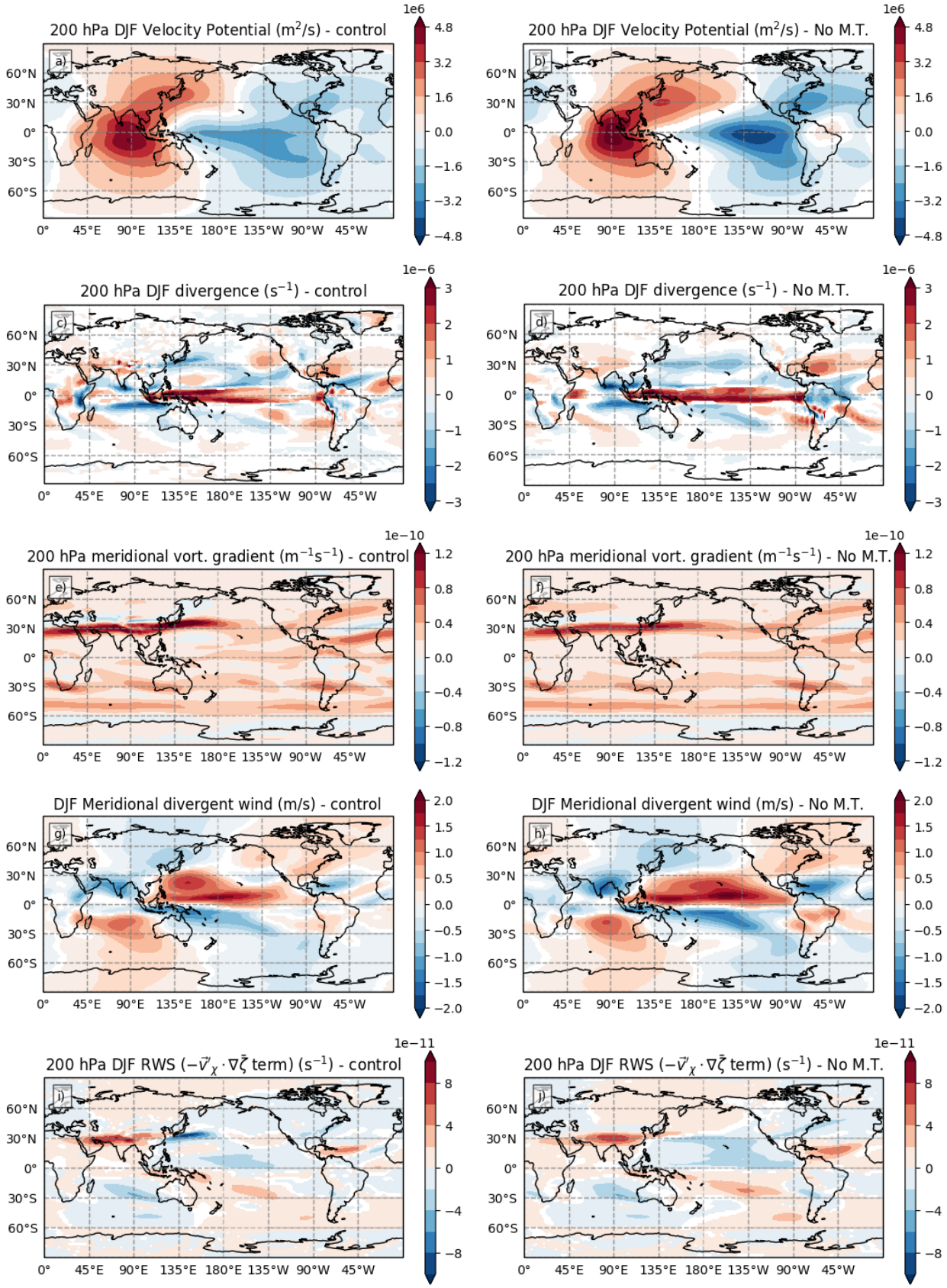

Figure 15: Subfigures a, b, c, d, g, h, i, and j are regressions against the PC1 time series. Only areas where the correlation is significant at the 95% level are plotted. Subfigures e and f are climatological DJF values.

ponent of the field. Negative values in the upper troposphere indicate upper-level divergence, which is a sign that upward motion is occurring below. Therefore, the negative χ centers in Fig.(15) (a, b) are areas of enhanced convection, whereas the positive χ centers indicate areas of upper-level convergence and suppressed convection. In both simulations, the area of warm SSTs in the tropical Pacific coincides with an area of negative anomalous velocity potential indicating enhanced convection. This large area of upwelling air west of the Date Line is balanced by an area of subsidence over the Indian ocean and South-East Asia, closing an overturning cell known as the Walker circulation.

The velocity potential is more strongly negative in the tropical Pacific area and more strongly positive over the Indian ocean in the NO_MT simulation. This indicates greater high-level divergence and convergence in those regions, which would be caused by the enhanced convection due to more intense SST anomalies.

Regressions of the upper-level divergence field (Fig.(15), c and d) allow us to see smaller-scale details.We see that there is a band of upper-level divergence along the equator in the Pacific ocean, which extends from the South American coast to the Indonesia. Two upper-level convergence areas appear at about 90°E in the NH and SH tropical regions, about 10° from the Equator. These are present in both simulations but stronger and more well-defined in the NO_MT case. As explained above, those areas of anomalous upper-level divergence act as a Rossby wave source. The exact location where the Rossby wave train emerges can clue us into the dynamics of the resulting teleconnection pattern, and thus a difference in Rossby wave source may explain the differences between the simulations.

An expression for the Rossby wave source can be derived by applying the vorticity equation at an upper tropospheric level and neglecting terms associated with vertical advection, twisting and friction (*Sardeshmukh and Hoskins* 1988):

$$\left(\frac{\partial}{\partial t} + \vec{v}\cdot\nabla\right)\zeta = -\zeta D, \tag{2}$$

where ζ is the absolute vorticity and D is the divergence. By separating the wind velocity into its irrotational and divergent components as in 1, we obtain:

$$\left(\frac{\partial}{\partial t} + \vec{v}_\psi\cdot\nabla\right)\zeta = -\vec{v}_\chi\cdot\nabla\zeta - \zeta D \tag{3}$$

The right-hand term is the total Rossby wave source, RWS. Sardeshmukh and Hoskins made a case for not assuming that the divergent component of the wind is negligible, even though it is smaller than the rotational component, because the advection of vorticity by both components is comparable as the divergent wind tends to be perpendicular to absolute vorticity contours. Therefore there are two main terms for the RWS as in 3: a term associated with vortex stretching and a term associated with the advection of vorticity by the divergent wind:

Breaking down the variables into their time-mean ($\bar{x}$) and anomalous (x') components, the expression for the RWS becomes:

$$\text{RWS} = -\vec{v'}_\chi\cdot\nabla\bar{\zeta} - \bar{\vec{v}}_\chi\cdot\nabla\zeta' - \bar{\zeta}D' - \zeta'\bar{D}, \tag{4}$$

Vortex stretching due to anomalous divergence is important in generating a Rossby wave source in the central Pacific about 15° poleward of the equator, which forces a Rossby wave that then propagates poleward and eastward giving rise to a teleconnection pattern (*Trenberth et al.* 1998). However, since vorticity advection by the divergent wind can also be important contributor, and given the importance of the meridional vorticity gradient in the region of the subtropical jet, we compute the anomalous Rossby Wave Source due to the mean vorticity advection by the anomalous divergent wind, $-\vec{v'}_\chi\cdot\nabla\bar{\zeta}$, to see if any contributions associated with this term are different between simulations.

The meridional and zonal components of the divergent wind are of the same magnitude, but the mean zonal vorticity gradient is at least one order of magnitude smaller than the meridional gradient, so the meridional advection contributes most to the Rossby Wave Source. Although the meridional vorticity gradient, shown in Fig.(15) e and f, is similar for both simulations and even stronger in the region of the jet stream for the CTL simulation, this is compensated for by v_χ, Fig.(15) (g, h), which is more strongly negative in that region for NO_MT.

Subplots i and j in Fig.(15) show the anomalous Rossby wave source due to the anomalous advection of time-mean vorticity by the anomalous divergent wind, which is the first term in Eq.4. For the NO_MT simulation there is a well-defined area of positive RWS in South Asia that may explain the Rossby wave train emerging from that area and propagating poleward. An area of positive RWS appears to also be present in the CTL simulation near the same location, although it is not as clearly defined. It is also noteworthy that the important area of negative Rossby wave source south of Japan in the CTL simulation is not present at all in the NO_MT simulation, as the meridional divergent wind is near-zero in that region.

Last of all, we briefly examine impact of the mountains on the surface pressure field. Fig.16 and Fig.17 show the sea level pressure anomaly field associated with El Niño for the CTL and NO_MT simulations. Comparing them with Fig.(8) allows us to see the baroclinic structure of the disturbances in the tropical Pacific, where the anomalies change sign with height, and the equivalent barotropic structure in the extratropics. The main difference between the simulations at this level is the northward displacement of the low in the north Pacific, as also seen to occur at higher levels.

IV. CONCLUSIONS

In this preliminary study we have found that the Tibetan and Mongolian Plateaus in central Asia greatly

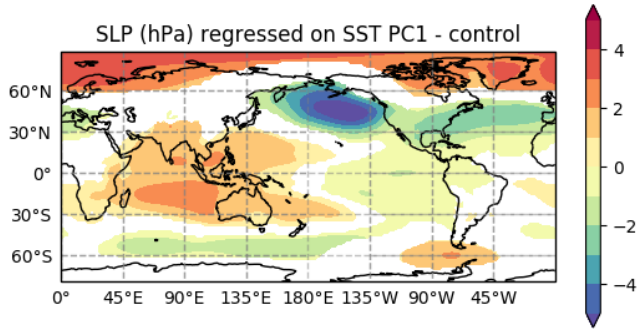

Figure 16: Regression of 200 hPa geopotential height anomalies against the PC1 time series for tropical SST for the CTL simulation. Areas where the correlation is significant at the 95% level are shaded.

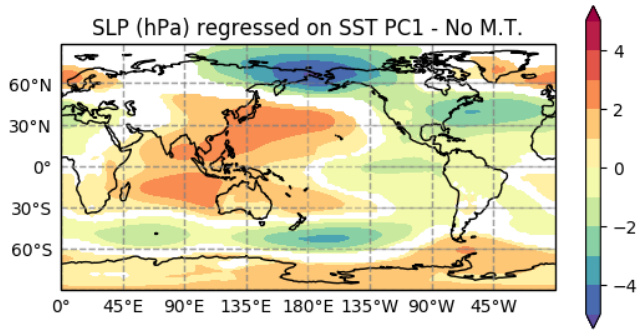

Figure 17: Regression of sea level pressure anomalies against the PC1 time series for tropical SST for the NO_MT simulation. Only areas where the correlation is significant at the 95% level are plotted.

influence not only the extra-tropical teleconnection patterns associated with the ENSO cycle, but also the temporal characteristics the oscillation itself. EOF analysis and spectral analysis have shown that the presence of the Asian orography in this model modifies the amplitude, regularity and periodicity of ENSO. The El Niño events in the NO_MT run exhibit more intense SST anomalies, a higher frequency with a shorter life cycle, and remarkably increased regularity. Results from recent studies suggest that these findings could be related to the influence of Asian orography on shorter scale events such as the Madden-Julian Oscillation and westerly wind bursts (*Yang and Wang* 2019), which are one of the possible causes of the irregularity of the ENSO cycle.

In the extratropics, the absence of mountains greatly alters the structure of the ENSO teleconnection pattern and adds a new wave train that appears to result from the anomalous upper-level divergence over the Indian subcontinent acting as a Rossby wave source. We therefore conclude that the Asian orography is critical for shaping the observed Northern Hemisphere winter teleconnections associated with ENSO SST anomalies in the equatorial Pacific Ocean.

Further research is needed to confirm these findings and establish the dynamical mechanism through which the Tibetan and Mongolian Plateaus contribute to the irregularity of the ENSO cycle and how they influence its extratropical teleconnection patterns. For example, analysis of weekly- or daily-scale low-level wind standard deviation in similar simulations could help determine whether changes in westerly wind events are related to the changes in ENSO regularity.

ACKNOWLEDGMENTS

I would like to thank my advisor, Dr. Ileana Bladé, for her invaluable guidance and help throughout the development of this Master's Thesis. I would also like to thank Dr. Rachel White of the Barcelona Supercomputing Center for all of the model data used in this work, as well as for the meaningful discussion and ideas that she and Dr. Javier García-Serrano have provided.

This work is dedicated to my family and friends, who have shown me limitless support throughout the years.

REFERENCES

Bolin, B., On the influence of the earth's orography on the general character of the westerlies, *Tellus*, *2*(3), 184–195, doi:10.3402/tellusa.v2i3.8547, 1950.

Capotondi, A., P. D. Sardeshmukh, and L. Ricciardulli, The nature of the stochastic wind forcing of enso, *Journal of Climate*, *31*(19), 8081–8099, doi:10.1175/JCLI-D-17-0842.1, 2018.

Held, I. M., M. Ting, and H. Wang, Northern winter stationary waves: Theory and modeling, *Journal of Climate*, *15*(16), 2125–2144, doi:10.1175/1520-0442(2002)015<2125:NWSWTA>2.0.CO;2, 2002.

Horel, J., and J. Wallace, Planetary-scale atmospheric phenomena associated with the southern oscillation, *Monthly Weather Review*, *109*, 813–829, doi:10.1175/1520-0493(1981)109<0813:PSAPAW>2.0.CO;2, 1981.

Hoskins, B. J., and D. J. Karoly, The steady linear response of a spherical atmosphere to thermal and orographic forcing, *Journal of the Atmospheric Sciences*, *38*(6), 1179–1196, doi:10.1175/1520-0469(1981)038<1179:TSLROA>2.0.CO;2, 1981.

Kestin, T. S., D. J. Karoly, J.-I. Yano, and N. A. Rayner, Time–frequency variability of enso and stochastic simulations, *Journal of Climate*, *11*(9), 2258–2272, doi:10.1175/1520-0442(1998)011<2258:TFVOEA>2.0.CO;2, 1998.

Kleeman, R., Stochastic theories for the irregularity of enso, *Philosophical Transactions of the Royal Society A: Mathematical, Physical and Engineering Sciences*, *366*(1875), 2509–2524, doi:10.1098/rsta.2008.0048, 2008.

Manabe, S., and T. B. Terpstra, The effects of mountains on the general circulation of the atmosphere as

identified by numerical experiments, *Journal of the Atmospheric Sciences*, *31*(1), 3–42, doi:10.1175/1520-0469(1974)031<0003:TEOMOT>2.0.CO;2, 1974.

Mo, K. C., and R. E. Livezey, Tropical-extratropical geopotential height teleconnections during the northern hemisphere winter, *Monthly Weather Review*, *114*(12), 2488–2515, doi:10.1175/1520-0493(1986)114<2488:TEGHTD>2.0.CO;2, 1986.

North, G. R., T. L. Bell, R. F. Cahalan, and F. J. Moeng, Sampling errors in the estimation of empirical orthogonal functions, *Monthly Weather Review*, *110*(7), 699–706, doi:10.1175/1520-0493(1982)110<0699:SEITEO>2.0.CO;2, 1982.

Rasmusson, E. M., and T. H. Carpenter, Variations in tropical sea surface temperature and surface wind fields associated with the southern oscillation/el niño, *Monthly Weather Review*, *110*(5), 354–384, doi:10.1175/1520-0493(1982)110<0354:VITSST>2.0.CO;2, 1982.

Sardeshmukh, P. D., and B. J. Hoskins, The generation of global rotational flow by steady idealized tropical divergence, *Journal of the Atmospheric Sciences*, *45*(7), 1228–1251, doi:10.1175/1520-0469(1988)045<1228:TGOGRF>2.0.CO;2, 1988.

Takahashi, K., and D. Battisti, Processes controlling the mean tropical pacific precipitation pattern. part i: The andes and the eastern pacific itcz, *J. Climate*, *20*, 3434–3451, doi:10.1175/JCLI4198.1, 2007.

Trenberth, K., and National Center for Atmospheric Research Staff, eds., The climate data guide: Nino sst indices (nino 1+2, 3, 3.4, 4; oni and tni)., `https://climatedataguide.ucar.edu/climate-data/nino-sst-indices-nino-12-3-34-4-oni-and-tni`, accessed: January 2020, 2018.

Trenberth, K., G. Branstator, D. Karoly, A. Kumar, N.-C. Lau, and C. Ropelewski, Progress during toga in understanding and modeling global teleconnections associated with tropical sea surface temperatures, *Journal of Geophysical Research*, *1031*, 14,291–14,324, doi:10.1029/97JC01444, 1998.

Wallace, J. M., and D. S. Gutzler, Teleconnections in the geopotential height field during the northern hemisphere winter, *Monthly Weather Review*, *109*(4), 784–812, doi:10.1175/1520-0493(1981)109<0784:TITGHF>2.0.CO;2, 1981.

White, R. H., D. S. Battisti, and G. H. Roe, Mongolian mountains matter most: Impacts of the latitude and height of asian orography on pacific wintertime atmospheric circulation, *Journal of Climate*, *30*(11), 4065–4082, doi:10.1175/JCLI-D-16-0401.1, 2017.

Wilks, D. S., *Statistical Methods in the Atmospheric Sciences*, 3rd ed., Oxford; Waltham, MA: Academic Press, 2011.

Yang, L. J., Y., and B. Wang, The tibetan plateau uplift is crucual for eastward propagation of madden-julian oscillation, *Scientific Reports*, *9*(15478), doi:10.1038/s41598-019-51461-w, 2019.